ACCEPTED MANUSCRIPT

Finite element analyses of human vertebral bodies embedded in polymethylmethalcrylate or loaded via the hyperelastic intervertebral disc models provide equivalent predictions of experimental strength

Yongtao Lu[a,*,1], Ghislain Maquer[b,1], Oleg Museyko[c], Klaus Püschel[d], Klaus Engelke[c], Philippe Zysset[b], Michael Morlock[a], Gerd Huber[a]

[a]Institute of Biomechanics, TUHH Hamburg University of Technology, Hamburg, Germany
[b]Institute of Surgical Technology & Biomechanics, University of Bern, Bern, Switzerland
[c]Institute of Medical Physics, University of Erlangen-Nuremberg, Erlangen, Germany
[d]Department of Legal Medicine, University Medical Center Hamburg-Eppendorf, Hamburg, Germany.
[1] The first two authors contributed equally to this work

Address of corresponding author:

Yongtao Lu Ph.D
Institute of Biomechanics
TUHH Hamburg University of Technology
Denickestraße 15
21073 Hamburg, Germany
Phone: +49 (0) 40 42878 3184
Fax: +49 (0) 40 42878 2996
Email:yongtao.lu@tuhh.de

Abstract: 249
Word count for the main text (Introduction to discussion): 2051
Number of tables: 2
Number of figures: 4

Abstract

Quantitative computer tomography (QCT)-based finite element (FE) models of vertebral body provide better prediction of vertebral strength than dual energy X-ray absorptiometry. However, most models were validated against compression of vertebral bodies with endplates embedded in polymethylmethalcrylate (PMMA). Yet, loading being as important as bone density, the absence of intervertebral disc (IVD) affects the strength. Accordingly, the aim was to assess the strength predictions of the classic FE models (vertebral body embedded) against the *in vitro* and *in silico* strengths of vertebral bodies loaded via IVDs. High resolution peripheral QCT (HR-pQCT) were performed on 13 segments (T11/T12/L1). T11 and L1 were augmented with PMMA and the samples were tested under a 4◦ wedge compression until failure of T12. Specimen-specific model was generated for each T12 from the HR-pQCT data. Two FE sets were created: FE-PMMA refers to the classical vertebral body embedded model under axial compression; FE-IVD to their loading via hyperelastic IVD model under the wedge compression as conducted experimentally. Results showed that FE-PMMA models overestimated the experimental strength and their strength prediction was satisfactory considering the different experimental set-up. On the other hand, the FE-IVD models did not prove significantly better (Exp/FE-PMMA: $R^2 = 0.68$; Exp/FE-IVD: $R^2 = 0.71$, $p = 0.84$). In conclusion, FE-PMMA correlates well with *in vitro* strength of human vertebral bodies loaded via real IVDs and FE-IVD with hyperelastic IVDs do not significantly improve this correlation. Therefore, it seems not worth adding the IVDs to clinical models until fully validated patient-specific IVD models become available.

Keywords: Human vertebra, finite element prediction, mechanical testing, failure strength, intervertebral disc

1. Introduction

Vertebral failure constitutes a serious health problem because of its association with back pain, disability and the impairment of life quality (Lips et al., 1999). The risk of vertebral failure is currently commonly determined by a wide range of bone mineral density (BMD) measurements, e.g. the areal BMD (aBMD) and the volumetric BMD (vBMD). However, studies showed only 50% to 70% of the variability in vertebral strength can be predicted by BMD measurements (Ammann and Rizzoli, 2003; Lochmüller et al., 2002). In order to improve the vertebral failure prediction, attention has been paid to other techniques, e.g. the finite element (FE) method, which can represent the bone microstructure not captured by the BMD measurements (Faulkner et al., 1991). Consequently, the FE modelling approach has recently gained increasing interest in predicting vertebral strength (Chevalier et al., 2010; Dall'Ara et al., 2012; Imai et al, 2008) and has shown better failure prediction than aBMD (Wang et al., 2012) and vBMD (Crawford et al., 2003) alone.

The vertebral strength was only assessed using vertebral bodies, whose endplates were either removed or embedded in polymethylmethacrylate (PMMA) to avoid uncertainties regarding the degree of degeneration of the elderly intervertebral disc (IVD) (Buckley et al., 2007; Crawford et al., 2003; Dall'Ara et al., 2012). These boundary conditions, although equivalent (Maquer et al. 2012a),

are not appropriate for the study of failures in vertebral endplate, which is a major failure pattern in the elderly (Rao and Singrakhia, 2003). On the other hand, the failure mechanisms in the vertebra are altered in the absence of IVD (Hussein et al., 2013), which plays an important role in transferring and distributing the compressive load (Adams et al., 2006). Moreover, the IVD stiffness affects the overall ductility of the vertebral bodies (Nekkanty et al., 2010) and the vertebral failure site (Pollintine et al., 2004). Finally, numerical simulations showed that FE models of embedded vertebral body provided different strength and failure patterns compared to models bonded to healthy IVDs (Maquer et al., 2012b). Accordingly, the aim of this study was to investigate whether the classic vertebral body embedded axial compression FE models (referred as FE-PMMA models) are still valid for the prediction of *in vitro* strength of human vertebral body loaded via IVDs under a wedge compression and if the predictions can be improved using FE spinal models with hyperelastic IVDs and *in vitro* consistent loading (FE-IVD models).

2. Materials and methods

2.1. *In vitro* mechanical testing

In this study, 13 T11/T12/L1 spinal segments, without failure, nor osteophytes, were received. The donors were postmenopausal females with a mean age of 79.9 ±

7.9 years [range: 67-90]. DXA bone densitometry (Lunar Prodigy, Lunar Corporation, Madison, WI, USA) was performed for the lumbar spine and both proximal femurs and subsequently all donors were diagnosed with osteoporosis according to the World Health Organization definition with a lumbar or femoral T-score of -2.5 or less. The segments were scanned while frozen using a HR-pQCT scanner (XtremeCT, Scanco Medical AG, Brüttisellen, Switzerland) with an image voxel size of 82 μm^3.

Following the standard procedures (Skrzypiec et al., 2013), the specimens were stored and prepared for mechanical testing. The spinal facet joints were removed for the loading to be only transferred via the IVDs. Failures in T11 and L1 were avoided by replacing the cancellous bone with PMMA (Technovit 4004, Heraeus Kulzer, Wehrheim, Germany). The specimens were embedded in metal cups, such that the mid-transverse planes of T12 were horizontal and in neutral posture (no bending).

The embedded specimens were mounted in a computer-controlled servo-hydraulic materials testing machine (MTS Bionix 858.2, Eden Prairie, MN, US). Axial force was applied for 15 min as a preconditioning to account for the post-mortem swelling (Hongo et al., 2008). The applied force was subject-specific and calculated based on the donor's body weight (300 N for a 70 kg person in standing position) (Nachemson, 1966). After preconditioning, a 4° anterior-posterior wedge

was applied to T11 to induce a wedge fracture loading condition for T12 (Adams et al. 2006) (Figure 1). An x-y-table was installed between the wedge and the actuator to allow free translations in the transverse plane and so to prevent coupled shear loading during assembly.

A quasi static compression loading of 0.1 mm/s was then applied (Brinckmann et al., 1989) and the x-y-table was locked to prevent extensive spinal anterior-posterior movements, eventually leading to rupture between the posterior regions of the IVD and the vertebral body. The test was performed until a dramatic drop of force (>15% of the peak force) was observed on the load-displacement curve. The maximal force measured was defined as the vertebral failure load (F^{exp}).

2.2. Finite element model

Subject-specific FE models of T12 vertebral bodies were created based on the HR-pQCT data. T11 and L1 were not modelled as their deformations were negligible due to PMMA augmentations. T12 models were created using an in-house software (MedTool, Institute of Lightweight Design and Structural Biomechanics, Vienna University of Technology, Vienna, Austria) (Pahr and Zysset, 2008). Quadratic wedge (C3D15) and tetrahedral elements (C3D10) were defined for the cortex and the trabecular bone, respectively, as described in Maquer et al. (2012b). The anisotropic elastic-plastic-damage model from Schwiedrzik and Zysset (2013) was

chosen to simulate the mechanical behaviour of each bone elements based on the local bone content and trabecular morphology.

The solid volume for each IVD was extruded from the superior and inferior endplate surfaces of its adjacent vertebrae (HyperMesh, Version 11.0, Altair Engineering Inc., Troy, MI, USA). The endplate surfaces were extracted from the meshes of T12 or reconstructed from the automatic segmentation of T11 and L1 (MIAF-Spine, Institute of Medical Physics, University of Erlangen, Germany) (Mastmeyer et al., 2006). The IVD volume was discretized with C3D10 and then the elements were organised into annulus fibrosus (AF) and nucleus pulposus (NP) according to the transverse sectional view (Figure 2).

Two IVD materials were used to generate either the classical FE-PMMA models or the FE-IVD models (Figure 3). Hence, linear elastic modulus of 2300 MPa and Poisson's ratio of 0.3 [Heraeus Kulzer GmbH, Wehrheim, Germany] were applied to both NP and AF elements for FE-PMMA. For FE-IVD, Mooney-Rivlin model was defined for NP and fibre-reinforced hyperelastic model (Moramarco et al., 2010) was chosen for AF. The material parameters are $C_{10,}$ C_{01}, C_{20}, K_1, K_2 and D, where, $C_{10,}$ C_{01} and C_{20} are related to the ground substance; K_1 and K_2 are parameters characterizing the behaviour of the collagen fibres; D is the incompressibility modulus. Two families of fibres with the angulations of ± 30°

(relative to the transverse plane) (Cassidy et al., 1989) were defined in AF and both families were acting only in tension.

Three different grades of IVD degeneration (healthy, moderately and severely) were identified from the IVD transverse sectional view (Thompson et al., 1990) and simulated in FE-IVD models. It was assumed that IVD degeneration had no effect on AF material properties (Schmidt et al., 2007), which were taken from literature (Moramarco et al., 2010) (Table 1). The material properties for healthy NP were also taken from literature (Schmidt et al., 2007) (Table 1). The dehydration of NP was simulated by changing the incompressibility modulus, whose value was 0.0005 MPa^{-1} for healthy IVD and corresponded to that of AF for severely degenerated IVD (Rohlmann et al., 2006). The incompressibility modulus for moderately degenerated IVD was linearly interpolated (Rohlmann et al., 2006). The stiffening of NP was simulated by modifying the values of C_{10} and C_{01} (Schmidt et al., 2007).

The bone and AF constitutive laws were implemented into Abaqus (Version 6.12, Dassault Systemes SIMULIA Ltd, Providence, RI, USA) via user defined material subroutine. To simulate the axial compression on FE-PMMA models, the bottom nodes from the inferior PMMA block were fully constrained while an axial displacement of 4.0 mm was prescribed to the nodes of the superior PMMA layer. To mimic the experimental loading applied to FE-IVD models, the bottom nodes

from the inferior IVD were fully constrained. A 2-stage loading was conducted on the cranial nodes of the superior IVD: a first step consisting in a 4° forward bending was followed by an axial displacement of 4.0 mm to ensure failure of T12. Non-linear analyses were performed and the FE failure loads (F^{FE}_{PMMA} and F^{FE}_{IVD}) were computed as the maximal force.

2.3. Statistical analysis

A paired two-tailed t-test was used to compare the vertebral failure loads with the FE predictions. Regression equations, the coefficients of determination (R^2) and root mean squared errors (RMS) were computed for the linear correlations of the vertebral failure load with FE predictions (Crawford et al., 2003). Analyses were performed using PASW statistics 18.0 (SPSS Inc., Chicago, IL, USA) and the probability of type I error was set to $\alpha = 0.05$, i.e. $p < 0.05$ was considered statistically significant.

3. Results

Compared to the experimental failure loads, FE predicted loads were 12% lower in FE-IVD group (mean ± SD, 2.09 ± 0.48 kN vs. 1.84 ± 0.47 kN, $p = 0.005$) and 18% higher in FE-PMMA group (2.09 ± 0.48 kN vs. 2.46 ± 0.62 kN, $p = 0.002$) (Table 2). Both predicted failure loads were significantly correlated (FE-IVD/FE-PMMA: $R^2 = 0.94$) and showed similar correlation with the experimental vertebral strength

(Exp/FE-PMMA: R^2 = 0.68; Exp/FE-IVD: R^2 = 0.71) (Figure 4). No significant difference was detected between the absolute value of the residuals from the FE-IVD and FE-PMMA regression models (p = 0.84).

4. Discussion

The study confirmed that the PMMA embedding is providing a higher vertebral strength, which is probably because a larger portion of the load is carried by the cortex (Homminga et al. 2001, Maquer et al. 2012b). Yet, despite different loading conditions, the FE-PMMA models provided a satisfactory prediction of the failure loads of vertebral bodies under a 4◦ wedge compression via IVDs and showed the same predictive power as the FE-IVD models (R^2 = 0.68 vs. 0.71). FE-PMMA models are more reproducible by avoiding approximation regarding the degree of elderly IVD's degeneration (Dall'ara et al. 2012), computationally more efficient and ease of clinical implementation. This essentially indicates that FE-PMMA models are satisfactory (Buckley et al., 2006), although rigid boundary conditions are prescribed to the endplates and axial compression conducted. This agreed with Yang et al.'s (2012) study where it was found that a 5◦ forward flexion does not significantly affect the spatial distribution of stress within the vertebral body.

The hyperelastic IVD model, although reasonable for simulation of the kinematic of the spine (Moramarco et al. 2010), and the instantaneous response of IVD (Jones, et al., 2008), is hardly applicable to simulate the *in vitro* load transfer

to the endplates. Indeed, the accuracy of the vertebral strength predictions is highly dependent on the degree of simplification of those IVD models (Jones, et al., 2008).While the latest image-based bone models (Pahr, et al., 2012; Hosseini, et al., 2012) move towards patient-specific modelling (Gefen, 2012), such step is still to be taken regarding the IVD modelling. In this study, IVD shape was deduced from the endplates of the neighbouring vertebral bodies (Moramarco, et al., 2010; Homminga, et al., 2012). MRI is able to accurately capture the IVD morphology, but the IVD geometry in most FE models are idealised and rarely based on MRI data (Moramarco, et al., 2010; Schmidt, et al., 2007). The distinction NP/AF is hardly possible with degenerated IVDs (Ellingson et al. 2012). Moreover, discrete degrees of degeneration were simulated as commonly done in most degeneration schemes (Thompson et al. 1990, Pfirmann et al. 2001). Considering the range of alterations observed in moderately to highly degenerative IVDs and that the elderly IVDs in this study were likely having different degenerative levels, a discretization constitutes a considerable simplification. Quantitative MRI data correlates with the IVD's mechanical properties (Périé et al. 2006, Campana et al. 2011, Maquer et al. 2014) but such information have not been applied to an IVD model.

Hence, despite the small sample size, this study showed that the vertebral strength computed by FE-PMMA models correlated well with the *in vitro* strength of human vertebral bodies loaded via real IVDs. The FE-IVD models did not

significantly improve this correlation, probably due to a lack of patient-specific disc models. In conclusion, for clinical assessment of strength, it is probably not worth the trouble of adding the discs to vertebral body models until fully validated patient-specific IVD models become available.

Ethical approval

Ethical approval has been obtained from the Ethics Committee of the Hamburg Chamber of Physicians (PV3486).

Acknowledgement

This work was supported by the German Federal Ministry of Education and Research (BMBF) under Grant 01EC1005 and by the Swiss National Science Foundation (SNF), grant n°483 325230_147153. The authors would like to acknowledge Kay Sellenschloh and Matthias Vollmer for their help in the mechanical testing, Imke Fiedler for assisting in the FE sample studies, Dr. med Matthias Krause for performing the HR-pQCT scans, Prof. Michael Amling for the support with the ethics approval and Dr. Birgit Wulff for counselling the next of kin.

References:

Adams, M.A., Pollintine, P., Tobias, J.H., Wakley, G.K., Dolan, P., 2006. Intervertebral disc degeneration can predispose to anterior vertebral failures in the thoracolumbar spine. Journal of Bone and Mineral Research 21 (9), 1409–1416.

Ammann, P., Rizzoli, R., 2003. Bone strength and its determinants. Osteoporosis International 14 (S3), S13–18.

Brinckmann, P., Biggemann, M., Hilweg, D., 1989. Prediction of the compressive strength of human lumbar vertebrae. Clinical Biomechanics 4 (S2), 1–27.

Buckley, J.M., Leang, D.C., Keaveny, T.M., 2006. Sensitivity of vertebral compressive strength to endplate loading distribution. Journal of Biomechanical Engineering 128(5), 641– 646.

Buckley, J.M., Loo, K., Motherway, J., 2007. Comparison of quantitative computed tomography-based measures in predicting vertebral compressive strength. Bone 40 (3), 767–774.

Campana, S., Charpail, E., De Guise, J. A., Rillardon, L., Skalli, W., Mitton, D., 2011. Relationships between viscoelastic properties of lumbar intervertebral disc and degeneration grade assessed by MRI. Journal of the Mechanical Behavior of Biomedical Materials 4(4), 593-599.

Cassidy, J.J., Hiltner, A., Baer, E., 1989. Hierarchical structure of the intervertebral disc. Connective Tissue Research 23(1), 75-88.

Chevalier, Y., Quek, E., Borah, B., Gross, G., Stewart, J., Lang, T., et al., 2010. Biomechanical effects of teriparatide in women with osteoporosis treated previously with alendronate and risedronate: results from quantitative computed tomography-based finite element analysis of the vertebral body. Bone 46 (1), 41–48.

Crawford, R.P., Cann, C.E., Keaveny, T.M., 2003. Finite element models predict in vitro vertebral body compressive strength better than quantitative computed tomography. Bone 33 (4), 744–750.

Dall'Ara, E., Schmidt, R., Pahr, D., Varga, P., Chevalier, Y., Patsch, J., Kainberger, F., Zysset, P., 2010. A nonlinear finite element model validation study based on a novel experimental technique for inducing anterior wedge-shape fractures in human vertebral bodies in vitro. Journal of Biomechanics 43(12), 2374-2380.

Dall'Ara, E., Pahr, D., Varga, P., Kainberger, F., Zysset, P., 2012. QCT-based finite element models predict human vertebral strength in vitro significantly better than simulated DEXA. Osteoporosis International 23 (2), 563–572.

Ellingson, A.M., Mehta, H., Polly, D.W., Ellermann, J., Nuckley, D.J., 2013, Disc degeneration assessed by quantitative T2* correlated with functional lumbar mechanics, Spine 38(24), E1533-E1540.

Faulkner, K.G., Cann, C.E., Hasegawa, B.H., 1991. Effect of bone distribution on vertebral strength: assessment with patient-specific nonlinear finite element analysis. Radiology 179(3), 669-674.

Gefen, A., 2012. Patient-specific Modeling in Tomorrow's Medicine (Vol. 9). Springer.

Homminga, J., Weinans, H., Gowin, W., Felsenberg, D., & Huiskes, R. 2001. Osteoporosis changes the amount of vertebral trabecular bone at risk of fracture but not the vertebral load distribution. Spine, 26(14), 1555-1560.

Homminga, J., Aquarius, R., Bulsink, V. E., Jansen, C. T., Verdonschot, N., 2012. Can vertebral density changes be explained by intervertebral disc degeneration? Medical Engineering and Physics 34(4), 453-458.

Hongo, M., Gay, R.E., Hsu, J.T., Zhao, K.D., Ilharreborde, B., Berglund, L.J., et al., 2008. Effect of multiple freeze-thaw cycles on intervertebral dynamic motion

characteristics in the porcine lumbar spine. Journal of Biomechanics 41 (4), 916–920.

Hosseini, H. S., Pahr, D. H., Zysset, P. K., 2012. Modeling and experimental validation of trabecular bone damage, softening and densification under large compressive strains. Journal of the Mechanical Behavior of Biomedical Materials 15, 93-102.

Hussein, A.I., Mason, Z.D., Morgan, E.F., 2013. Presence of intervertebral discs alters observed stiffness and failure mechanisms in the vertebra. Journal of Biomechanics 46, 1683-1688.

Imai, K., Ohnishi, I., Yamamoto, S., Nakamura, K., 2008. In vivo assessment of lumbar vertebral strength in elderly women using computed tomography-based nonlinear finite element model. Spine 33 (1), 27–32.

Jones, A. C., Wilcox, R. K., 2008. Finite element analysis of the spine: towards a framework of verification, validation and sensitivity analysis. Medical Engineering and Physics 30(10), 1287-1304.

Lips, P., Cooper, C., Agnusdei, D., Caulin, F., Egger, P., Johnell, O., et al., 1999. Quality of life in patients with vertebral failures: Validation of the quality of life questionnaire of the European Foundation for Osteoporosis (QUALEFFO). Working Party for Quality of Life of the European Foundation for Osteoporosis. Osteoporosis International 10 (2), 150–160.

Lochmüller, E.M., Bürklein, D., Kuhn, V., Glaser, C., Müller, R., Glüer, C.C., et al., 2002. Mechanical strength of the thoracolumbar spine in the elderly: prediction from in situ dual-energy X-ray absorptiometry, quantitative computed tomography (QCT), upper and lower limb peripheral QCT, and quantitative ultrasound. Bone 31 (1), 77–84.

Maquer, G., Dall'Ara, E., Zysset, P. K., 2012a. Removal of the cortical endplates has little effect on ultimate load and damage distribution in QCT-based voxel

models of human lumbar vertebrae under axial compression. Journal of Biomechanics 45(9), 1733-1738.

Maquer, G., Schwiedrzik, J., Zysset, P.K., 2012b. Embedding of human vertebral bodies leads to higher ultimate load and altered damage localisation under axial compression. Comput Methods Biomech Biomed Engin. http://dx.doi.org/10.1080/10255842.2012.744400. (Epub ahead of print).

Maquer, G., Brandejsky, V., Benneker, L. M., Watanabe, A., Vermathen, P., Zysset, P. K., 2014. Human intervertebral disc stiffness correlates better with the Otsu threshold computed from axial T2 map of its posterior annulus fibrosus than with clinical classifications. Medical Engineering and Physics 36(2), 219-225.

Mastmeyer, A., Engelke, K., Fuchs, C., Kalender, W.A., 2006. A hierarchical 3D segmentation method and the definition of vertebral body coordinate systems for QCT of the lumbar spine. Medical Image Analysis 10, 560-577.

Moramarco, V., Perez del Palomar, A., Pappalettere, C., Doblare, M., 2010. An accurate validation of a computational model of a human lumbosacral segment. Journal of Biomechanics 43 (2), 334-342.

Nachemson, A., 1966. The load on lumbar disks in different positions of the body. Clinical Orthopaedics and Related Research 45, 107-122.

Nekkanty, S., Yerramshetty, J., Kim, D., Zauel, R., Johnson, E., Cody, D.D., et al., 2010. Stiffness of the endplate boundary layer and endplate surface topography are associated with brittleness of human whole vertebral bodies. Bone 47 (4), 783–789.

Pahr, D.H., Zysset, P.K., 2008. From high-resolution CT data to finite element models: development of an integrated modular framework. Computer Methods in Biomechanics and Biomedical Engineering 12 (1), 45–57.

Pahr, D. H., Dall'Ara, E., Varga, P., Zysset, P. K., 2012. HR-pQCT-based homogenised finite element models provide quantitative predictions of

experimental vertebral body stiffness and strength with the same accuracy as μFE models. Computer Methods in Biomechanics and Biomedical Engineering, 15(7), 711-720.

Perie, D., Iatridis, J. C., Demers, C. N., Goswami, T., Beaudoin, G., Mwale, F., Antoniou, J., 2006. Assessment of compressive modulus, hydraulic permeability and matrix content of trypsin-treated nucleus pulposus using quantitative MRI. Journal of Biomechanics 39(8), 1392-1400.

Pfirrmann, C. W., Metzdorf, A., Zanetti, M., Hodler, J., Boos, N., 2001. Magnetic resonance classification of lumbar intervertebral disc degeneration. Spine 26(17), 1873-1878.

Pollintine, P., Dolan, P., Tobias, J.H., Adams, M.A., 2004. Intervertebral disc degeneration can lead to 'stress-shielding' of the anterior vertebral body: a cause of osteoporotic vertebral failure? Spine 29 (7), 774–782.

Rao, R.D., Singrakhia, M.D., 2003. Painful osteoporotic vertebral failure: pathogenesis, evaluation, and roles of vertebroplasty and kyphoplasty in its management. The Journal of Bone and Joint Surgery American Volume. 85 (10), 2010–2022.

Rohlmann, A., Zander, T., Schmidt, H., Wilke, H.J., Bergmann, G., 2006. Analysis of the influence of disc degeneration on the mechanical behaviour of a lumbar motion segment using the finite element methods. Journal of Biomechanics 39 (13), 2484 -2490.

Schmidt, H., Kettler, A., Rohlmann, A., Claes, L., Wilke, H.J., 2007. The risk of disc prolapses with complex loading in different degrees of disc degeneration – A finite element analysis. Clinical Biomechanics 22 (9), 988–998.

Schwiedrzik, J.J., Zysset, P.K., 2013. An anisotropic elastic viscoplastic damage model for bone tissue. Biomechanics and Modeling in Mechanobiology 12 (2), 201–213.

Skrzypiec, D.M., Bishop, N.E., Klein, A., Pueschel, K., Morlock, M.M., Huber, G., 2013. Estimation of shear load sharing in moderately degenerated human lumbar spine. Journal of Biomechanics 46(4), 651-657.

Thompson, J.P., Pearce, R.H., Schechter, M.T., Adams, M.E., Tsang, I.K., Bishop, P.B., 1990. Preliminary evaluation of a scheme for grading the gross morphology of the human intervertebral disc. Spine 15 (5), 411–415.

Wang, X., Sanyal, A., Cawthon, P.M., Palermo, L., Jekir, M., Christensen, J., et al., 2012. Prediction of new clinical vertebral failures in elderly men using finite element analysis of CT scans. Journal of Bone and Mineral Research 27 (4), 808–816.

Yang, H., Nawathe, S., Fields, A.J., and Keaveny, T.M. 2012. Micromechanics of the human vertebral body for forward flexion. Journal of biomechanics, 45(12), 2142-2148.

Table 1. Material properties for different grades of intervertebral disc

		healthy	moderately degenerated	severely degenerated	Reference
nucleus pulposus	C_{10} [MPa]	0.12	0.17	0.19	(Schmidt et al. 2007, Rolhmann et al. 2006)
	C_{01}[MPa]	0.03	0.041	0.045	
	D [MPa^{-1}]	0.0005	0.158	0.3	
annulus fibrosus	C_{10} [MPa]	0.1			(Moramarco et al., 2010)
	C_{20} [MPa]	2.5			
	D [MPa^{-1}]	0.3			
	K_1 [MPa]	1.8			
	K_2	11.0			

Table 2. Donor information and failure load data for the 13 T12 vertebral bodies

Parameter	Mean ± SD	Range
Age [year]	79.9 ± 7.8	65 – 90
Body weight [kg]	54.9 ± 15.8	41 – 94.7
F_{IVD}^{FE} [kN]	1.84 ± 0.47	1.03 – 2.50
F_{PMMA}^{FE} [kN]	2.46 ± 0.62	1.39 – 3.40
F^{exp} [kN]	2.09 ± 0.48	1.01 – 2.73

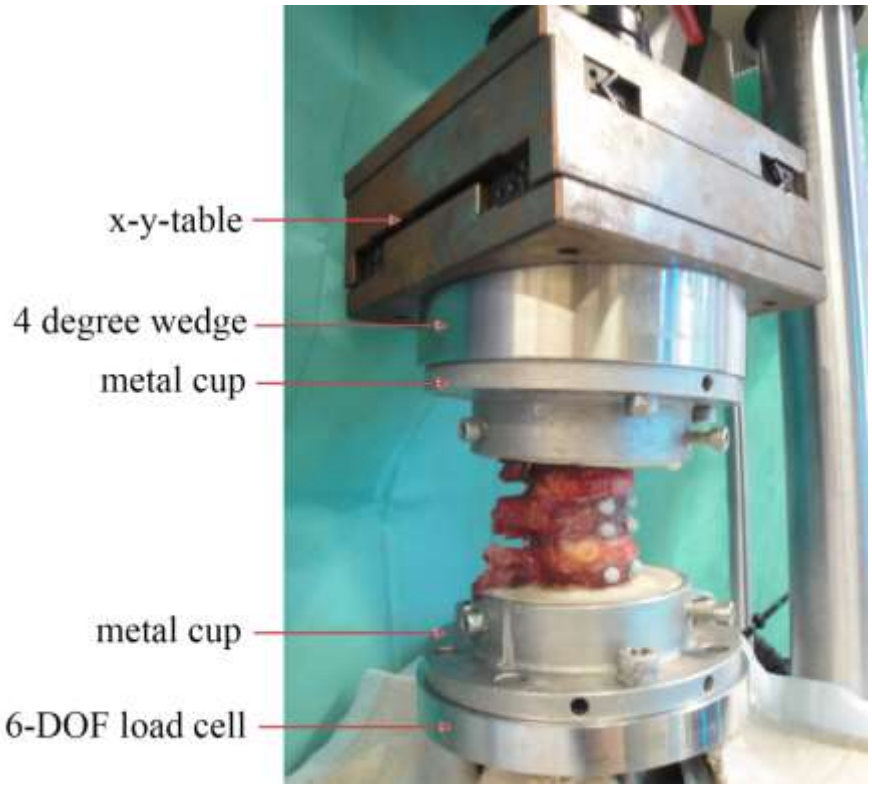

Figure 1. Mechanical testing setup for a representative 3-vertebra segment with disconnected facet joints.

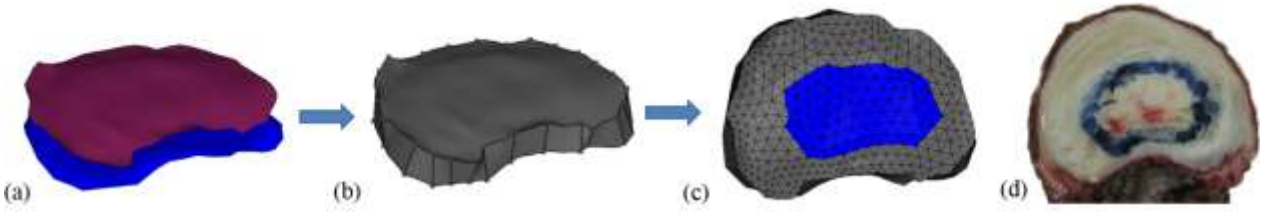

Figure 2. Generation of the finite element intervertebral disc (IVD) and comparison with the transverse sectional view of corresponding IVD, (a) surfaces extracted from its adjacent vertebrae, (b) IVD volume created from the two surfaces, (c) IVD meshes with annulus fibrosus (grey) and nucleus pulposus (blue), (d) transverse sectional view of the IVD (the boundary between the nucleus pulposus and annulus fibrosus was marked with blue ink).

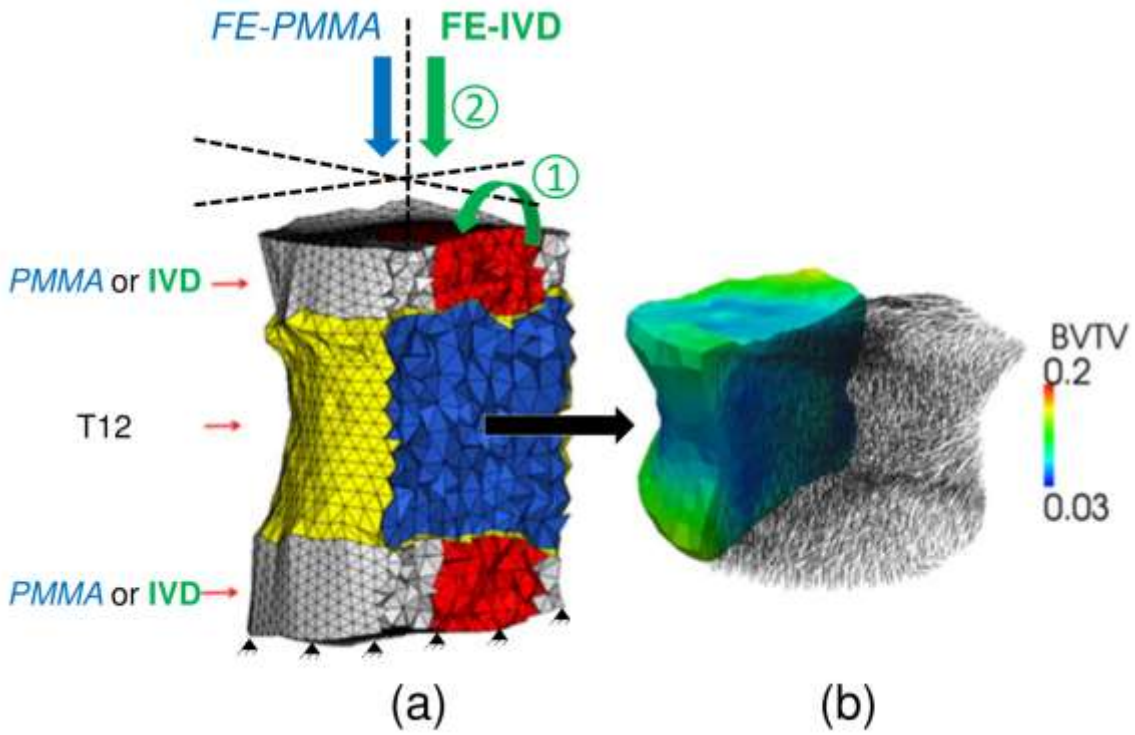

Figure 3. (a) Two boundary conditions were simulated for each T12 model: either pure axial compression was prescribed to the nodes of the superior *PMMA* layer (*FE-PMMA*) or a 2-stage loading (step 1: 4° forward bending, step 2: axial compression) was conducted to the nodes of the superior IVD (FE-IVD). In both cases, the bottom nodes of the model were fully constrained. Each T12 model was discriminated between 4 regions: HR-pQCT based cortical (yellow) and cancellous bone (blue), annulus fibrosus (grey) and nucleus pulposus (red). (b) Material heterogeneity of the cancellous bone of a T12 model with bone volume fraction (BV/TV) and fabric anisotropy.

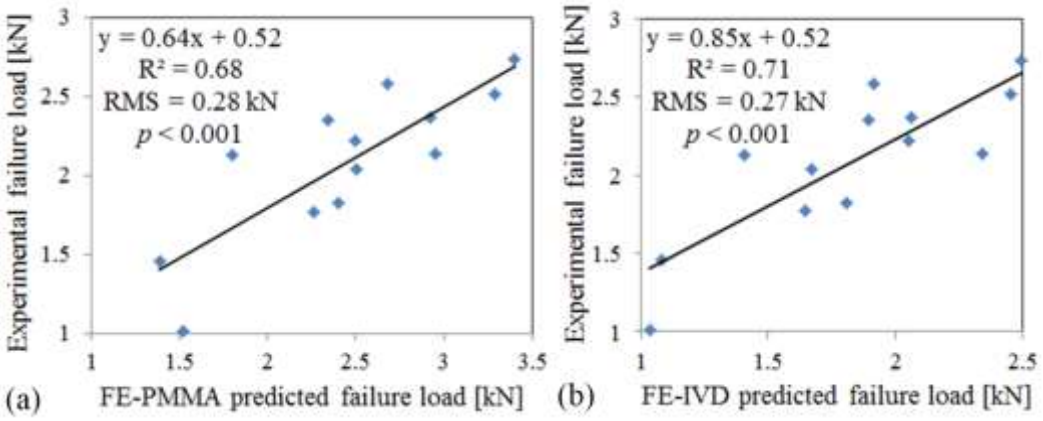

Figure 4. Linear regressions of the vertebral failure load as a function of the failure loads predicted by the FE-PMMA (a) and FE-IVD (b) models.